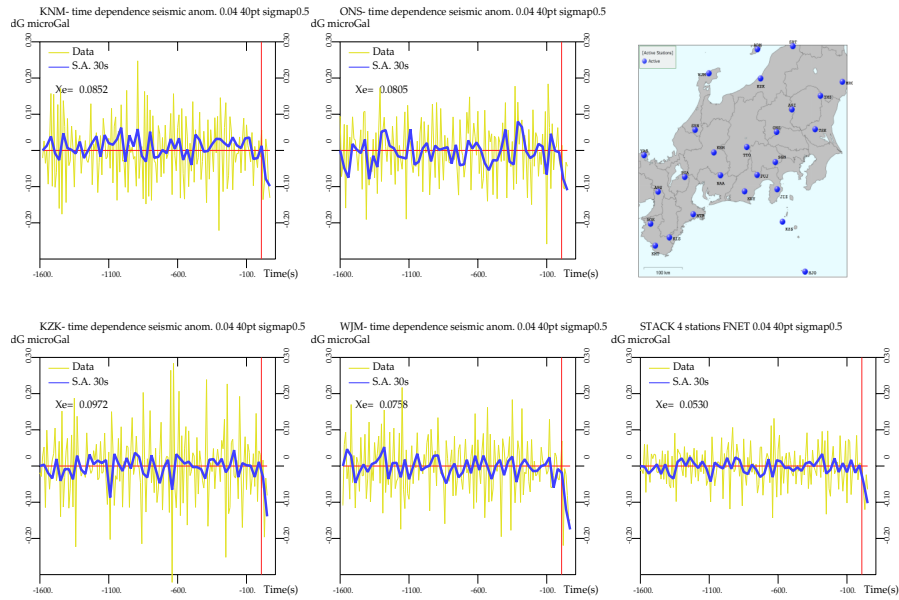
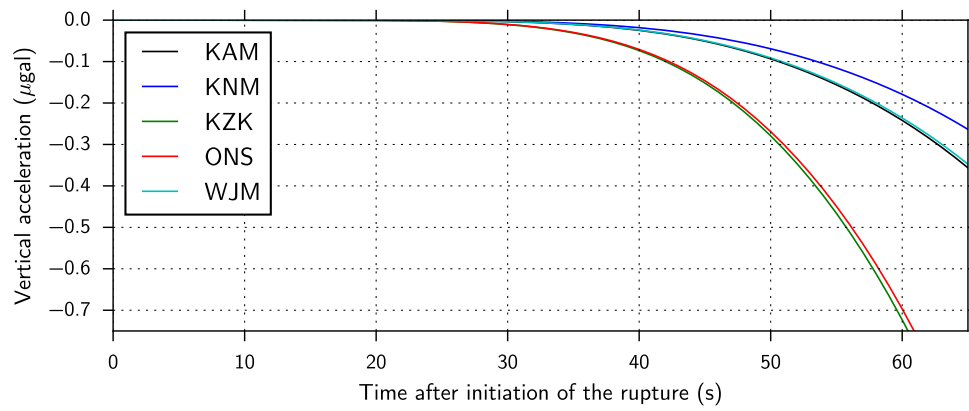


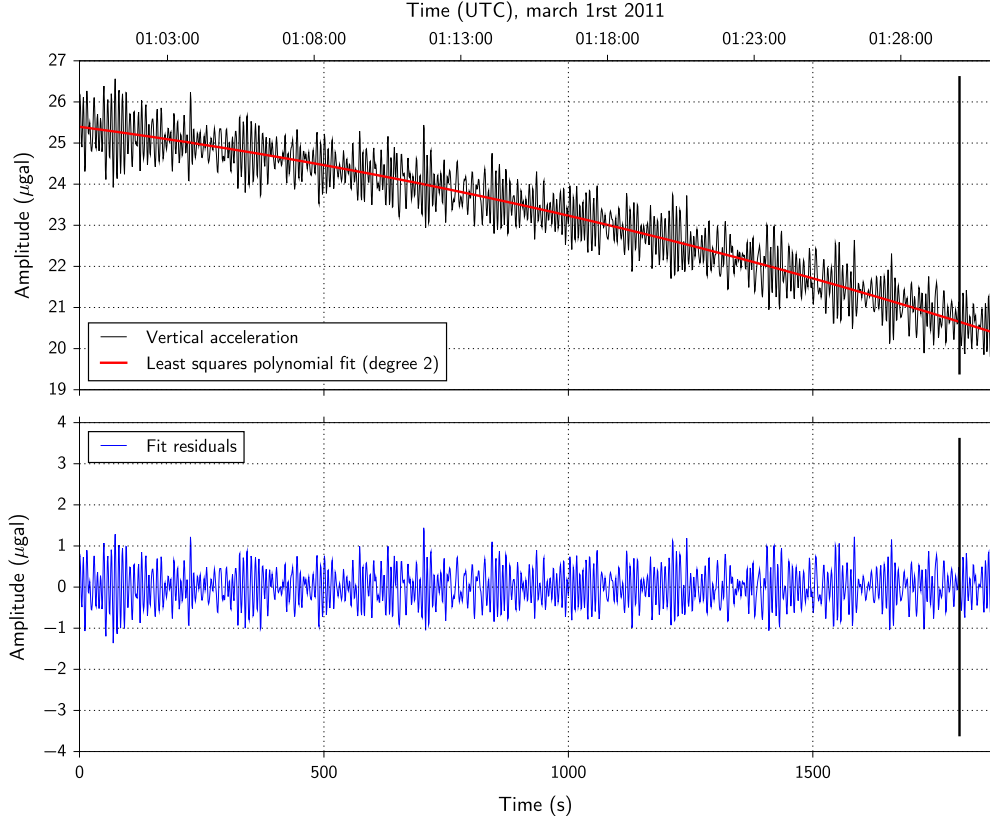
Supplementary Figure 1: Residuals of the Kamioka gravity data (yellow line) before the Tohoku event for different correlation times  $\Lambda$  from 400 s to 1000 s. The vertical red line corresponds to the rupture onset time,  $t_{eq}$ . P-waves arrive approximately at  $t_P = t_{eq} + 72$  s. The fitting curve is calculated up to  $t_{eq}$  and extrapolated analytically between  $t_{eq}$  and  $t_P$ . The upper and lower red curves indicate the *a posteriori* uncertainties (diagonal terms of the *a posteriori* covariance function of parameters). The horizontal scale is in seconds and the vertical scale in  $\mu\text{Gal}$  ( $10^{-8} \text{ m/s}^2$ ). Residuals smoothed by sliding average (S.A.) over 30 s are shown as a blue curve.



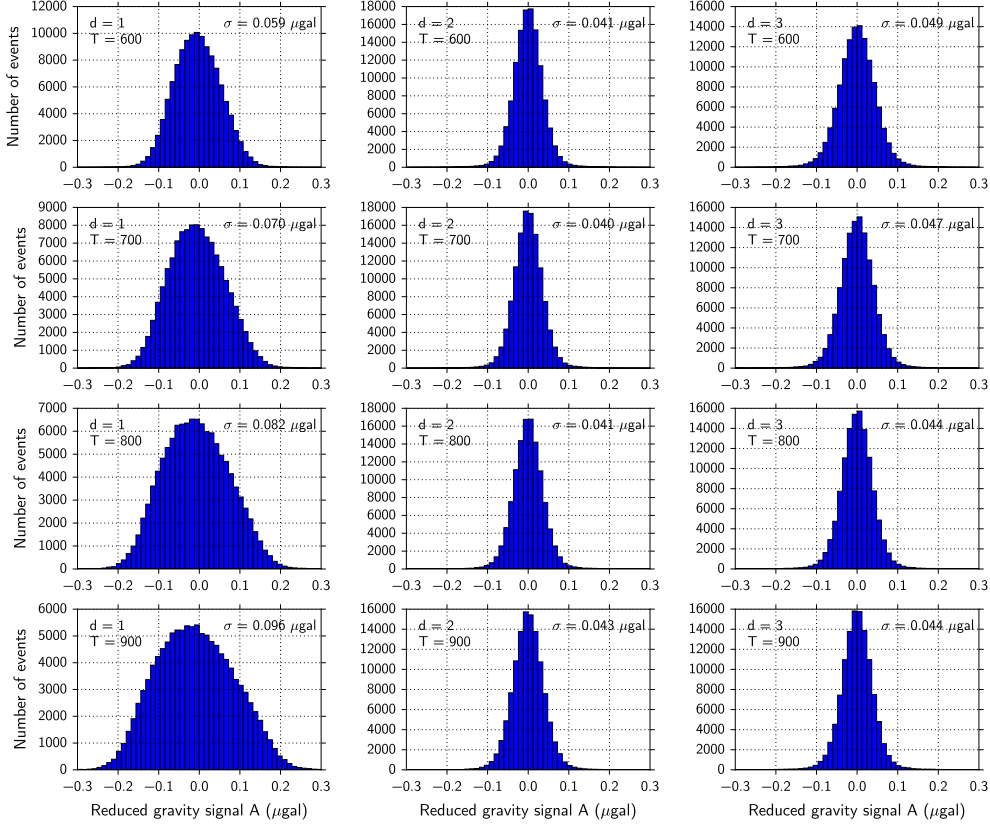
Supplementary Figure 2: Four left figures: yellow curves are residuals of vertical-component broadband seismograms at F-net stations KNM, ONS, KZK and WJM relative to the smoothed curve obtained by the method described above. The horizontal scale is in seconds and the vertical scale in  $\mu\text{Gal}$  ( $10^{-8} \text{ m/s}^2$ ). Blue lines are residuals filtered by a 30 s sliding average. Bottom right: residuals and smoothed residuals of the stack of the four seismograms. Top right: map of the F-net network.



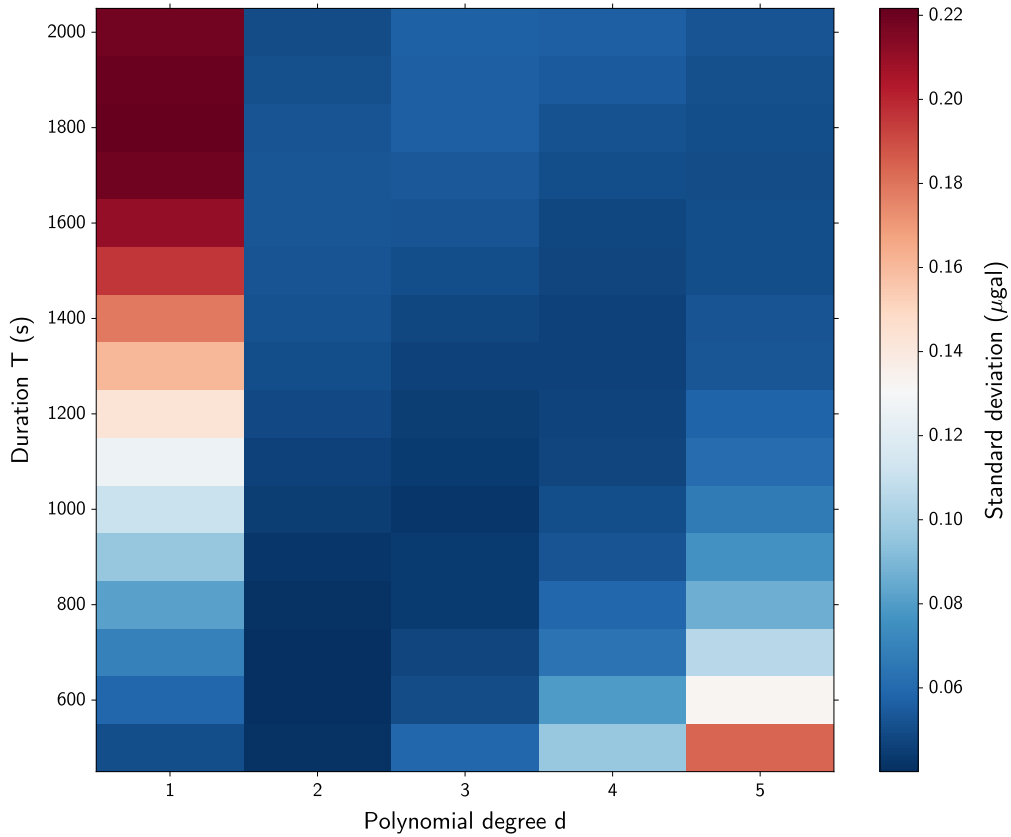
Supplementary Figure 3: Theoretical calculation of the gravity signal at different stations of F-net, KNM, KZK, ONS, WJM, and Kamioka gravimeter station KAM. The anti-alias filter described in the main text is applied, as in Figure 4(a).



Supplementary Figure 4: Example of signal detection method for a typical time interval. This figure shows that the signal is largely dominated by the microseismic noise, which is reduced by applying a 30 s-sliding average window. Top : Least squares polynomial fit (red) applied on a background time interval signal (black). In this example, the degree of the fitting polynomial is 2, and its coefficients are those that minimize the sum of squared errors in the 1800 seconds-long interval (up to the vertical line). Once the coefficients are determined, we extrapolate the fitting polynomial after the vertical line, for 65 seconds. Bottom : Fit residuals, i.e. the difference between the fitting polynomial and the vertical acceleration. If its standard deviation differs significantly from the standard deviation of the event interval  $\sigma_{\text{Tohoku}}$ , the corresponding time interval is rejected, and the reduced gravity signal  $\mathcal{A}$  is not computed. Defining  $\sigma$  as the standard deviation of the fit residuals up to the vertical line and  $\sigma_{extr}$  as its standard deviation after the vertical line, the interval is rejected if it fails to satisfy  $0.75 \sigma_{\text{Tohoku}} < \sigma < 1.25 \sigma_{\text{Tohoku}}$  and  $\sigma_{extr} < 10 \sigma_{\text{Tohoku}}$ .



Supplementary Figure 5: Distributions of the reduced gravity signals for the background data, as a function of the time window  $T$  and of the polynomial degree  $d$  used to fit the acceleration on background time intervals. The computation of the reduced gravity signal  $\mathcal{A}$  is performed for all the selected intervals. We explore the whole parameter space  $(T, d)$  but only some examples are displayed in this figure. For a given time window  $T$ , if  $d$  is too small, the fit cannot represent the complexity of the data, whereas if  $d$  is too large, its extrapolation diverges quickly. In both cases, the resulting  $\mathcal{A}$  distributions are broadened. Thus, for this rough parameter space exploration, the smallest variance of  $\mathcal{A}$  is obtained for  $d=2$  and  $T=700$  seconds (not far from the optimal parameter setting,  $d=2$  and  $T=690$ s, obtained with a more thorough, refined exploration).



Supplementary Figure 6: Standard deviation of the reduced gravity signals for background data, as a function of the time window duration  $T$  and the polynomial degree  $d$  used for the fit. The (rough) parameter space exploration extends the one presented in Supplementary Figure 5, the smallest variance of  $\mathcal{A}$  is still obtained for  $d=2$  and  $T=700$ s.

# 1 Supplementary Methods

## 2 Preliminary analysis of gravimetric and seismic datasets

3 A preliminary analysis of the gravimetric and broadband seismic data was  
4 performed by fitting the data  $x(t)$  by a slowly varying continuous function  
5  $f_{synt}(t)$ , up to  $t_{\text{end}}$ , and then extrapolating  $f_{synt}(t)$  after  $t_{\text{end}}$  up to the arrival  
6 of P-waves. We adopt the Bayesian fitting approach described by [1], which  
7 avoids side effects such as acausal signal and ringing phenomena, and requires  
8 the choice of a correlation time  $\Lambda$  of the noise and a fitting interval  $T$ . The  
9 errors on the fit can be derived from the diagonal terms of the *a posteriori*  
10 covariance function of parameters.

### 11 - Kamioka dataset

12 The differences between data and fit are shown in Supplementary Figure 1 for  
13  $\Lambda$  ranging from 400 s to 1000 s and for  $T = 2000$  s. The data are decimated  
14 to a sampling rate of 0.1 Hz in order to mitigate the microseismic noise and to  
15 enhance the low frequency components. The residuals are largely dependent  
16 on the choice of  $\Lambda$ . They can be as large as  $-0.2 \mu\text{Gal}$  for the shortest  $\Lambda$ , and  
17 decrease as  $\Lambda$  increases. We smoothed the residuals by applying a sliding  
18 average window of 30 s, which further reduces the microseismic noise. The  
19 averaged residual (blue line) is in the range  $-0.15$ - $0.1 \mu\text{Gal}$ , slightly larger  
20 than other anomalies before  $t_{\text{end}}$ , but the result is largely dependent upon  
21 the choice of the correlation time  $\Lambda$  and the fitting time  $T$ .

22 This preliminary search suggests the presence of a signal, but is not suf-  
23 ficient to assess a statistical significance. Since the number of independent  
24 parameters is not defined in the fitting method, in order to be independent of  
25 the choice of the fitting parameters, we designed the *blind* statistical analysis  
26 described in the main text. The statistical analysis uses polynomial functions  
27 to fit the slow trend, for the sake of simplicity and computational efficiency.  
28 The blind analysis with polynomials is different and independent from the  
29 preliminary analysis.

### 30 - Broadband seismic data of the Japanese network F-net

31 We consider the broadband seismic data of four stations close to Kamioka  
32 with the best signal-to-noise ratio. They are processed with the same method

33 described above, with a correlation time of 400 s. Since we look for an instan-  
34 taneous gravity effect (no propagation), we stack these data to improve the  
35 signal-to-noise ratio (Supplementary Figure 2). The theoretical predictions  
36 as in the main text are presented in Supplementary Figure 3.

### 37 **Blind statistical analysis of the Kamioka dataset**

38 Two steps of the blind statistical detection procedure are illustrated for the  
39 Kamioka records in Supplementary Figures 4 to 6. The blind test in the main  
40 text, for Kamioka and F-net seismic stations at similar epicentral distances  
41 follows the same procedure.

## 42 **Supplementary References**

- 43 [1] Tarantola, A. & Valette, B. Generalized nonlinear inverse problems  
44 solved using least squares criterion. *Rev. Geophys. Space Phys.* **20**, 219–  
45 232 (1982).